Geoderma 239–240 (2015) 115–129

Contents lists available at ScienceDirect

Geoderma

journal homepage: www.elsevier.com/locate/geoderma

Landscape-scale exploratory radiometric mapping using proximal soil sensing

U. Stockmann *, B.P. Malone, A.B. McBratney, B. Minasny

Soil Security Laboratory, Department of Environmental Sciences, Faculty of Agriculture and Environment, The University of Sydney, Suite 401, Biomedical Building C81, 1 Central Avenue, ATP, Eveleigh, NSW, Australia

ARTICLE INFO

Article history:
Received 10 July 2014
Received in revised form 29 September 2014
Accepted 4 October 2014
Available online 10 October 2014

Keywords:
Gamma radiometrics
Regional exploratory geophysical survey
Proximal soil sensing
Regression kriging

ABSTRACT

The soil's gamma radiometric signal is known to be a crucial indicator of the heterogeneity of soil properties, most likely directly related to the mineralogy and geochemistry of the parent material. However, fine-resolution radiometric data sourced from geophysical surveys are often not available. In our study area in the Lower Hunter Valley, Australia, only coarse-scale (based on 2 km line spacing) aerial radiometric maps are available. An alternative solution could be to implement a 'smart' ground-based gamma-ray survey when detailed radiometric information is required on larger extent. The work presented here therefore details a vehicle-borne gamma-ray soil survey conducted in the Lower Hunter Valley to investigate if a proximal soil sensing device with a footprint much smaller than airborne gamma-ray spectrometers can be employed for regional extent mapping, and still capture the soil's fine-scale heterogeneity. To do so we designed an algorithm for the delineation of irregular transects (drive-lines) based on ancillary environmental information, intended to be used specifically for Wide-Ranging Exploratory Surveys (WIRES) at the regional scale. The WIRES algorithm creates transects from randomised starting points that terminate at boundary points; the path is defined with directional constraints that collectively ensure that the environmental variability within the domain of study is accessed and sampled. The design was delineated for the entire 220 km^2 study area. In this exploratory work we surveyed a sub-catchment of the area ($\approx$15 km^2) to trial the feasibility of WIRES. We produced radiometric maps based on a regression-kriging approach. An external validation of the maps showed good results. We also validated the maps produced with existing detailed radiometric maps across a landholding ($\approx$140 ha) that is situated within the sub-area investigated in this study. Both surveys were comparable, which gives us useful insights into understanding the scaling properties of the geophysical properties of soil across environments.

1. Introduction

On-the-go proximal soil sensing techniques are an invaluable resource to resolve spatially, a number of environmental phenomena. Such information can enrich our knowledge of the variability of soil landscapes across a location of interest. The resulting fine-resolution environmental data are often used as ancillary information for digital soil mapping to provide the necessary 'environmental' information to spatially predict soil characteristics.

One of the on-the-go proximal soil sensing instruments that has been utilised for geophysical surveys over the past decades have been passive gamma-ray spectrometers. These record the amount of radioactive isotopes in the soil based on the principle that each gamma ray photon relates to a discrete energy window which is characteristic of the source isotope (Minty et al., 1998). Radiometric mapping therefore predominantly reflects the variation of the amount of naturally occurring radioisotopes of potassium (^{40}K), uranium (^{238}U-series) and thorium (^{232}Th-series) as they produce high-energy gamma-rays with sufficient intensities to be picked up by the detector (IAEA, 2003). Gamma rays emitted from the soil correspond to the concentration of these radioisotopes in the top 40 cm of soil (Wilford et al., 1997). Generally, their intensity is directly related to the mineralogy and geochemistry of the parent material and its degree of weathering (Dickson and Scott, 1997). Radiometric surveys, mainly aerial-based, have therefore been used initially for uranium exploration and geological mapping on a large scale (Wilford and Minty, 2006). But these geophysical surveys have also been utilised more frequently over the years to map soils and regolith distribution and in turn to understand soil landscape processes on a regional scale.

More explicitly, radiometric maps have been used successfully to detect the spatial variation of soil across the landscape, in relation to soil-forming materials and to distinguish between the intensity of weathering of the material (Cook et al., 1996; Wilford, 2012; Wilford and Minty, 2006). They have also been employed to improve our understanding of soil erosion and deposition in the landscape by mapping the occurrence of the man-made radioisotope ^{137}Cs in surface soils (Scheib and Beamish, 2010; Stockmann et al., 2012). In addition, radiometric data have been used to identify site-specific soil properties when

* Corresponding author.
E-mail address: uta.stockmann@sydney.edu.au (U. Stockmann).

http://dx.doi.org/10.1016/j.geoderma.2014.10.005
0016-7061/

calibrated with field data such as Aeolian dust additions to topsoil (Cattle et al., 2003), soil texture and Fe contents of the surface soil (Viscarra Rossel et al., 2007), and absence or presence of gravel (Taylor et al., 2002). Radiometric information of the soil landscape is therefore a crucial explanatory variable of the heterogeneity of soil properties in digital soil mapping efforts (McBratney et al., 2003). However, even though radiometric information is seen as a highly valuable asset for improving the prediction of the soil's spatial distribution, radiometric data are often not readily available continuously at a fine resolution across a wide range of spatial scales.

Whilst Australia has a continental coverage of remotely-sensed radiometric data at a nominal resolution of 100 m, it is composed of a patchwork of aerial surveys that range in information content (Minty et al., 2009). For example, flight line spacing could be as little as 100 m or greater than 1500 m (Percival, 2010). Where detailed aerial survey has been completed, the radiometric data is invaluable for digital soil mapping. Conversely, where coarse aerial survey (2 km line spacing) has been completed, as in our study area of the Lower Hunter Valley (around 32.83°S 151.35°E), Australia the radiometric information content is low and consequently is unable to capture local soil heterogeneities. In addition, financial cost is the main primary impediment for conducting a user-specified detailed aerial or ground-based survey in the entire study area of the Hunter Wine Country Private Irrigation District (HWCPID). An alternative solution to this however could be to implement a ground-based or vehicle-borne gamma-ray survey when detailed radiometric information is required on the regional scale (up to 30 km^2). Recently, Viscarra Rossel et al. (2014) conducted a gamma radiometrics survey along widely separated transects using a mobile proximal soil sensor over a 100 km^2 region in Tasmania and the resulting radiometric maps appeared to accord well with ancillary information of the surveyed region. However, to survey a location of interest efficiently with a vehicle-borne spectrometer, an optimal drive-line route is required that (ideally also) takes ancillary environmental information into account. This is relatively simple to implement for a small landholding (up to ~100 ha) where surveying is based on closely-spaced parallel driving lines of 10–30 m in width (McBratney and Pringle, 1999). In precision agriculture, RAVEN navigation devices (Raven industries, Sioux Falls, South Dakota, USA) are used for example to navigate and to ensure overlapping drive lines coverage of the surveyed area. In addition, Geographic Information Systems such as ESRI's ArcGIS offer the shortest or optimum path algorithms that advise on best driving routes along pathways but in general cannot be used when off-road sampling transects are required. These also take no existing environmental information of the area of interest into account.

The work presented in this study explicitly details a vehicle-borne gamma-ray soil survey conducted in the Lower Hunter Valley to investigate if a ground-based proximal soil sensing device with a footprint much smaller than airborne gamma-ray spectrometers can be employed for regional extent mapping, and still capture the soil's heterogeneity. The difference in footprint sizes is predominantly a function of altitude from the soil surface. To do so we designed a 'sampling' algorithm that creates irregular transects throughout a region for 'optimal' off-road navigation through the landscape based on ancillary environmental information that is intended to be used specifically for Wide-Ranging Explanatory Surveys (WIRES) at the regional scale.

2. Materials and methods

2.1. WIRES — an algorithm for Wide-Ranging Exploratory (soil) Surveys

We designed an algorithm for automatically generating drive-line transects called WIRES, which is an acronym for WIde-Ranging Exploratory (soil) Survey. A figurative meaning of the algorithm is the arrangement and bending of wires across a landscape. The algorithm is a custom-built function computed using the R programming language (R Development Core Team, 2008) that can be made available upon request. To generate one transect, the WIRES algorithm follows the general format:

1) Define the area to be surveyed with an outline polygon. Make a configuration of *m* points across the land area to be surveyed. The selection of points could follow any type of sample design, for example, simple random or stratified simple random designs (de Gruijter et al., 2006), or even conditioned Latin Hypercube sampling (Minasny and McBratney, 2006).
2) Form a Delaunay triangulation of these points. Fig. 1 shows a contrived example of 25 random points and the subsequent triangulation of these.
3) Select a point at random without replacement. In Fig. 1, this point is labelled *A*. Points on the convex hull of the configuration are however not permitted to be sampled, as these form the termination sites of a formed transect and are labelled *X* on the second plot. The vertices of the outline polygon then form the terminals of the transects.
4) Determine the nearest point to *A* at random. In Fig. 1, this point is labelled *B*.
5) Form a triangle *ABC* with the neighbouring points of *B*. In Fig. 1 there are 3 neighbouring points: *C1*, *C2*, and *C3*.
6) Select the neighbouring point which maximises the angle at *B* which ensures a maximum projected distance away from point A to avoid path repetition. Using measured distances and cosine rules, the selected neighbouring point on the example is *C2*.
7) Transect is drawn following the triangulation lines from point *A*, through *B*, to point *C*. Point *B* is now labelled new point *A*, and point *C* is now labelled new point *B*.
8) Go back to step 5, and repeat until point *C* becomes one of the termination sites, which marks the end of a transect. The final transect can be seen on the second plot of Fig. 1.
9) Go back to step 3 to generate more than one transect.

There is a maximum to how many transects can be created for a given number of point locations. This number is generally *m* minus the number of convex hull points. It is not necessary to know the number of convex hull points, as the standard procedure is to instruct WIRES to generate *n* transects, and let the algorithm run until it terminates (there are no more *A* points to sample). After this, a filtering step is performed to remove redundant transects, those which are identical to another transect. With the remaining transects, a random sample (without replacement) of size *n* (for example an integer which is 10% of *m* may be a useful rule of thumb) is taken. This sampled composition of transects constitute the proposed survey design of a given area under study. By fact or nature of the design, there will be situations where the route of a particular transect will follow (and not just intersect), for some part, the route of another. The consideration here is that each transect is unique, but if overlapping of transects becomes apparent at any stage, it is only required to explore the overlapping route once.

2.2. Study area

We implemented and tested the WIRES algorithm for the creation of drive-line transects of 100 m or more in width for regional extent gamma-radiometric mapping in the Lower Hunter Valley, NSW, Australia. This area of study covers approximately 200 km^2 and encompasses the localities of Pokolbin and Rothbury (32.83°S 151.35°E) which are approximately 140 km north of Sydney, NSW, Australia (Fig. 2). The study area is situated in a temperate climatic zone, and experiences warm humid summers, and relatively cool yet also humid winters, receiving on average, just over 750 mm of rainfall annually.

The underlying geology is predominantly Early Permian, with some Middle and Late Permian formations (Fig. 3). Detailed reviews and additional maps of the geology can be found in Hawley et al. (1995). The soils across the study area, or composition thereof is quite variable, but in general terms are weathered kaolinitic and smectitic soils, of light to medium clay textures. The dominant soil groups are Luvisols

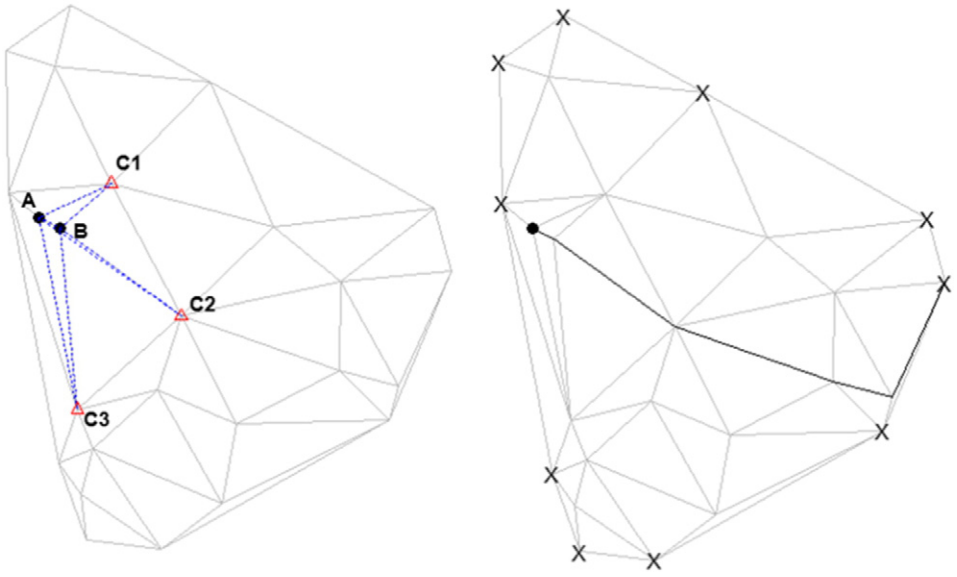

Fig. 1. These plots show the Delaunay triangulation based on 25 randomly placed points. The first plot diagrammatically shows the selection of points *A* (random point selection), *B* (nearest neighbour of *A*), and *C* (point at which maximises the angle at *B* from a formed triangle of the three points). Here there are 3 possible points, but *C2* meets the criteria best. A transect is drawn and algorithm continues until a convex hull point (*X*) is reached, and then terminates (second plot).

and on topographic high Calcisols (IUSS Working Group WRB, 2007). Further information regarding the soils can be found in Kovac and Lawrie (1991) and Malone et al. (2011). Landuse across the study area is predominantly composed of dryland agricultural grazing systems, followed by an expansive viticultural industry. Whilst most of the land has been dedicated for these uses, tracts of remnant natural vegetation

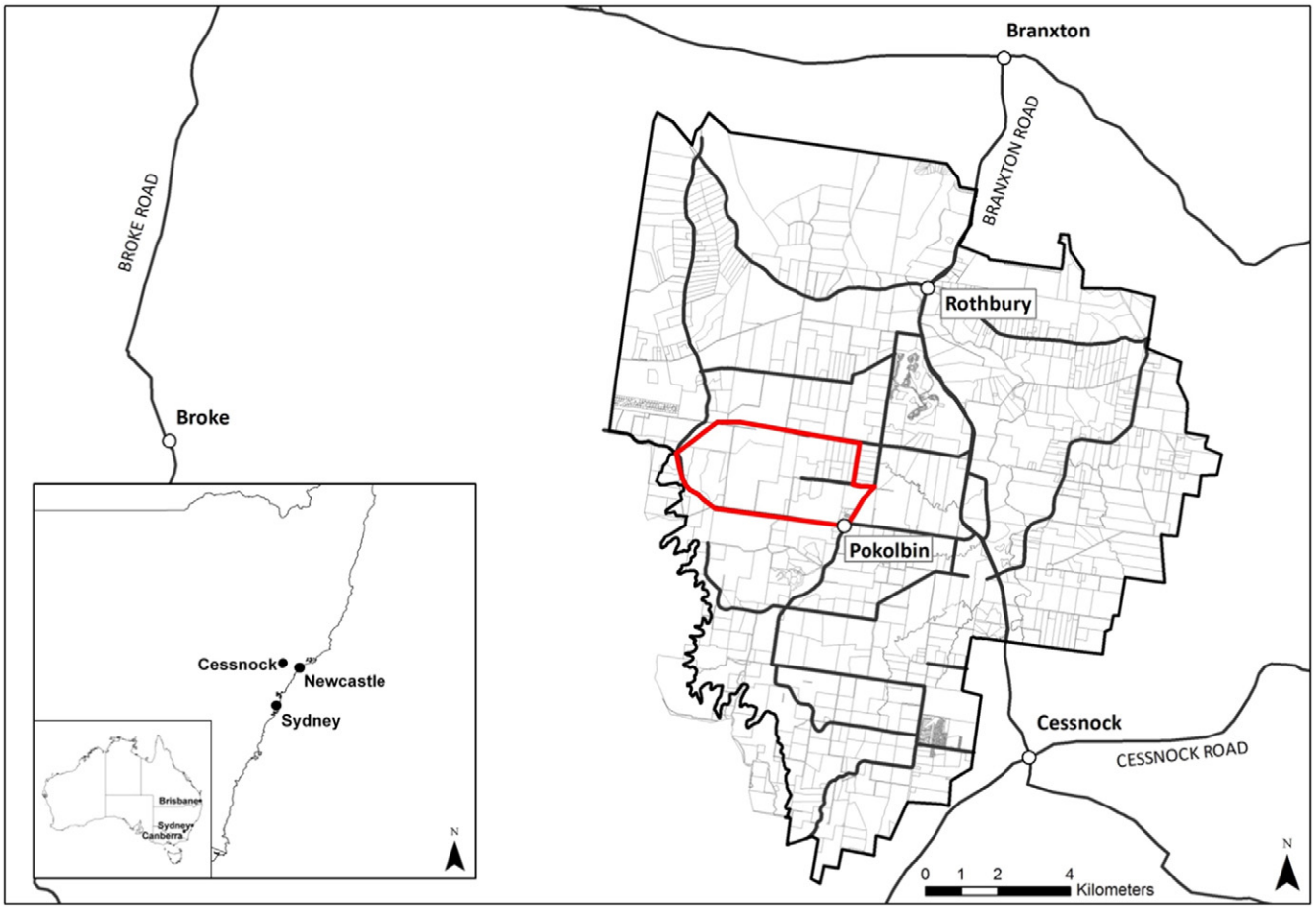

Fig. 2. Hunter Wine Country Private Irrigation District (HWCPID) study area in respect to its location in New South Wales (large box) and Australia (small box). The location of the regional-scale radiometrics survey is also shown (red outline).

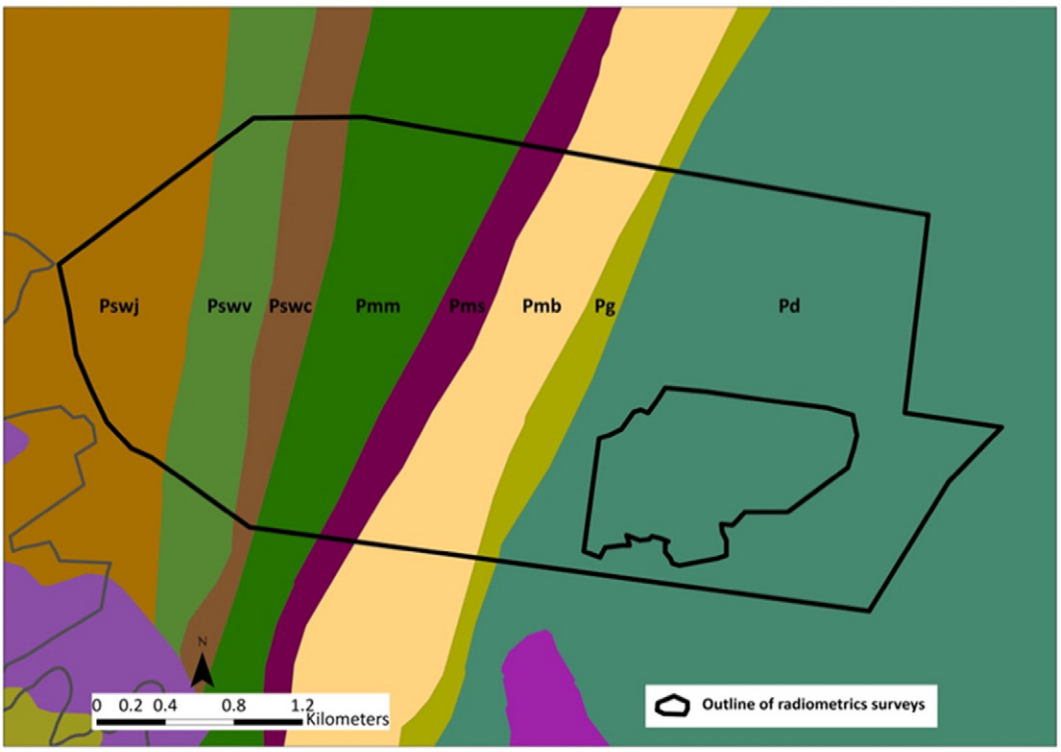

Era	Period		Stratigraphy			Symbol		Lithology	
PALAEOZOIC	PERMIAN	Late	Singleton Supergroup	*Wollombi Coal Measures*	Glen Gallic Subgroup	Psl		Coal seams, claystone (tuffaceaous) siltstone, sandstone, conglomerate	
					Doyles Creek Subgroup				
					Horseshoe Creek Subgroup				
					Apple Tree Flat Subgroup				
					Watts Sandstone			Medium to coarse-grained sandstone	
				Wittingham Coal Measures	Denman Formation	Pswj		Sandstone, siltstone	
					Jerrys Plains Subgroup			Coal seams, claystone, tuff, siltstone, sandstone, conglomerate	
					Archerfield Sg	Pswv		Well sorted quartz, lithic sandstone	
					Vane Subgroup			Coal seams, siltstone, lithic sandstone, shale, conglomerate	
					Saltwater Creek Formation	Pswc		Sandstone, siltstone, minor coaly bands	
		Middle	Maitland Group	*Mulbring Siltstone*		Pmm		Siltstone, claystone, minor fine-grained sandstone	
				Muree Sandstone		Pms		Fine to coarse-grained sandstone, conglomerate	
				Branxton Formation		Pmb		Conglomerate, sandstone, siltstone	
		Early	Greta Coal Measures	*Rowan Formation*	*Greta Coal Measures*	Pgr	Pg	Coal seams siltstone, sandstone	Coal seams, siltstone, sandstone
				Skeletar Formation		Pgk		Pellet claystone, siltstone, chert	
			Dalwood Group	Gyarran Volcanics Py	*Farley Formation*	Pd	Pdf	Rhyollite, acid to basic volcanics and volcanics and pyroclastics	Silty sandstone
					Rutherford Formation		Pdr		Siltstone, minor sandstone and marl
					Allandale Formation		Pda		Conglomerate, lithic sandstone
					Lochinvar Formation		Pdl		Basalt, siltstone, sandstone

Fig. 3. Geology units of the regional-scale survey area (Source: Hunter Coalfield Regional 1:100,000 Geology Map (Glen and Beckett, 1993)).

(dry sclerophyll forest) are apparent, particularly towards the south-western area which is bordered by Broken Back Range, Werakata National Park situated to the east, and some areas situated in the northern extents.

2.3. Implementation of the WIRES algorithm

We based our selection of number of points used in WIRES on the size of our study area (Hunter Valley Wine Country Private Irrigation

District — HWCPID) and the average landholding or parcel size. Based on a cadastral layer of the study area, the average parcel size was identified to be approximately 0.1 km^2 (10 ha). To establish a point configuration we assumed a sampling density as being equal to: A/N, where A is the size of the study area of about 200 km^2 and N is the average parcel size of 0.1 km^2 — thus the sample point configuration was set to 2000 points. Our intention next was to arrange the configuration of points across the area in an appropriate manner. For this we performed conditioned Latin Hypercube sampling (Minasny and McBratney, 2006) of size m (2000) of a number of environmental covariates, namely digital maps of 25 m pixel resolution. The following covariates were used in the sampling design: eastings and northings, elevation, landcover classification (Stabile, 2011), compound topographic index (SAGA Geographic Information System), a soil drainage index (Malone et al., 2012), mapping of marl presence (Malone et al., 2014), clay content of the subsoil (Malone et al., 2014), pH of the subsoil (Malone et al., 2014), and gamma radiometric total count (originally at 250 m resolution; Minty et al., 2009). With the cLHS, the algorithm optimises the sampling to ensure that the full distribution of each variable used is adequately sampled. The result being that the entire (known) environmental space will be sampled.

With the configuration of points arranged, the WIRES algorithm was set to generate 2000 transects (Fig. 4). After the algorithm terminated, redundant transects were removed, then a random sample (without replacement) of 200 was taken. These 200 transects collectively formed the design of the survey intended for measuring and subsequent mapping of gamma radiometrics across the study area (Fig. 4).

2.4. Ground-based radiometric survey

As detailed previously, the design of the ground-based survey was delineated for the entire 200 km^2 study area of the HWCPID. We surveyed a sub-catchment of the area of approximately 15 km^2 which is underlain by a range of differing geological units (refer to Fig. 3) to trial the feasibility of WIRES (Fig. 5).

The radiometric survey was carried out in autumn 2013 using a vehicle-borne RSX-1 gamma detector consisting of a 4 dm^3 Sodium–Iodine crystal (Radiation Solutions Inc., Mississauga, Ontario, Canada), and mounted on a six-wheeled field vehicle. Positional data were recorded with an integrated Trimble GPS. As seen in Fig. 6, it was necessary to adjust the vehicle path in the field, on-the-go, because of obstacles in the pathway of the delineated WIRES transects (such as fences, buildings, dense forest areas and water bodies) as well as restricted access to some of the properties falling within our study area. Although constrained by the requirement to adjust drive-lines on-the-go, we succeeded in covering most of the WIRES-delineated transects throughout the regional-scale study area. We also collected additional radioelement measurements on any necessary detours from the delineated driving lines as we captured the information continuously instead of only taking measurements once we arrived at a drive-line transect or node.

The RSX-1 collects a spectrum at 1 Hz using 1024 channels of 3 keV width in the range of 0 to 3000 keV. Radiometric information (Regions Of Interest of the Total Count, Potassium, Uranium and Thorium) was derived using the integrated software of the gamma spectrometer (RadAssist, Version 3.13, Radiation Solutions Inc.). ROI outputs were pre-processed to eliminate outlier sampling points employing Principal Component Analysis (PCA) for outlier detection based on Mahalanobis distance as outlined in Filzmoser and Reimann (2003). After outlier removal, the sampling density of the regional-scaled survey equated to 45 sampling points per hectare with a range in drive-line spacing of 80–650 m. To reduce the sampling size or number of point-based soil observations used in the digital soil mapping approach, we divided our study area into a regular grid of 5 m pixels, followed by the delineation of one radiometric measurement for every 5 m pixel by calculating the mean of the radiometric point measurements falling onto that particular 5 m pixel.

2.5. Radiometric mapping and measures of quality assessment

We generated radiometric maps of the regional-scale survey, showing the spatial distribution of the Total Counts (TC, cps), Potassium (K, cps), Uranium (U, cps) and Thorium (Th, cps) based on a regression

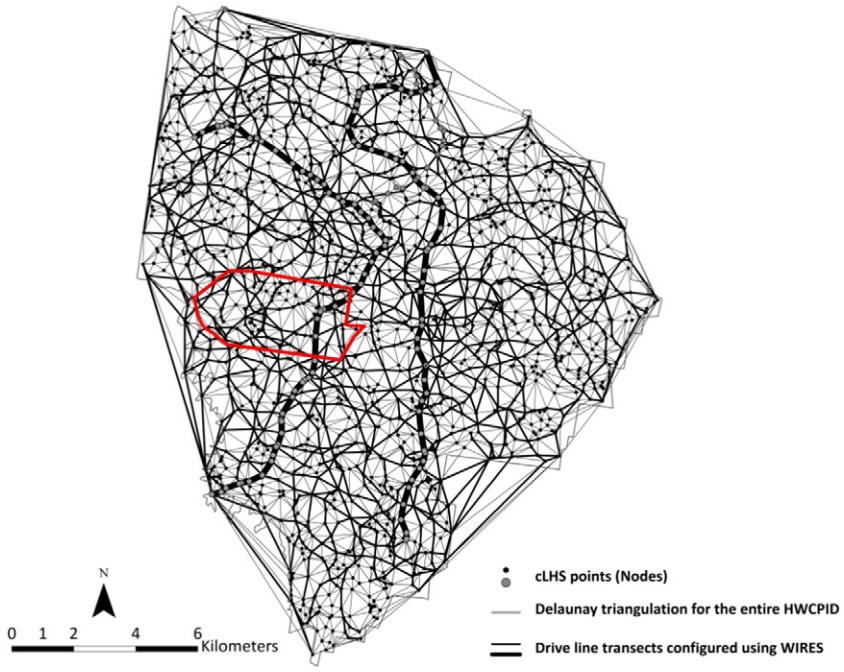

Fig. 4. Map of the HWCPID study area, showing the conditioned Latin Hypercube Sampling (cLHS) point configuration (2000 points or nodes), Delaunay triangulation based on cLHS points as well as the selected transects (200 transects). Two of the 200 delineated transects are highlighted here to demonstrate the length and delineation of the WIRES transects in the HWCPID study area. The location of the regional-scale radiometrics survey is also shown (red outline).

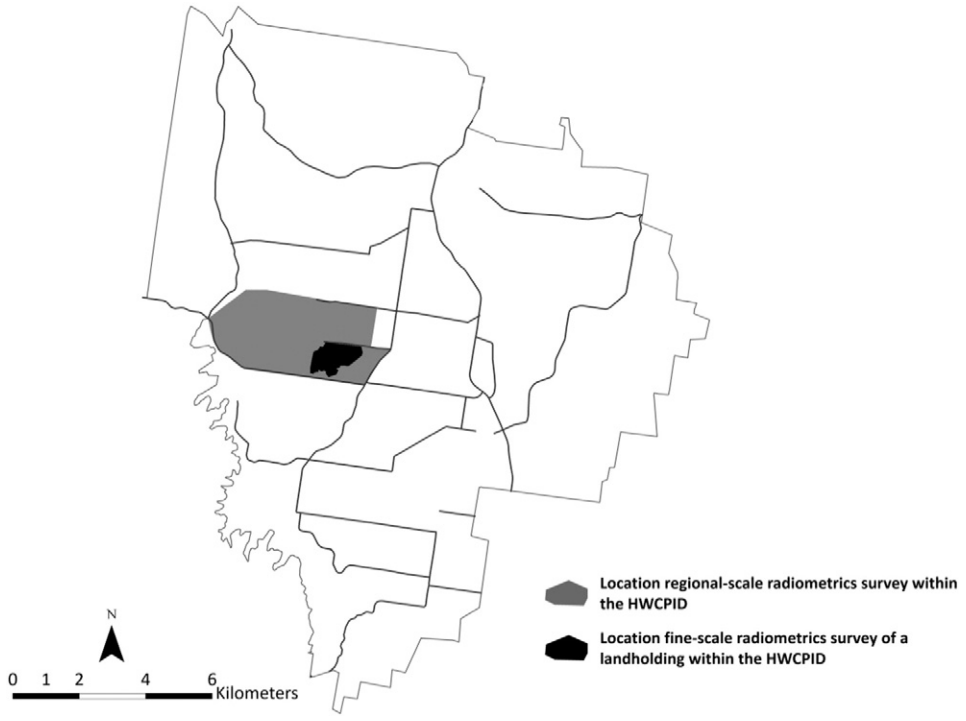

Fig. 5. Location of the regional-scale radiometric survey as well as the fine-scale radiometric survey within the HWCPID.

kriging modelling approach (McBratney et al., 2003). We chose regression kriging as it is a common prediction method in digital soil mapping that utilises all local (environmental) information available. Its prediction performance has also been demonstrated to perform best when compared to for example co-kriging approaches (Odeh et al., 1995). We used step-wise multiple linear regression where the target variables at each point along the WIRES transects (ROI) were modelled against a suite of environmental covariates determined from 25 m rasters of terrain attributes and soil physical and chemical properties (refer to Table 1). Model equations determined using this approach were extrapolated on a regular 25 m grid that encompasses the total extent of the regional-scale survey area. Assuming that the mean of the residuals of

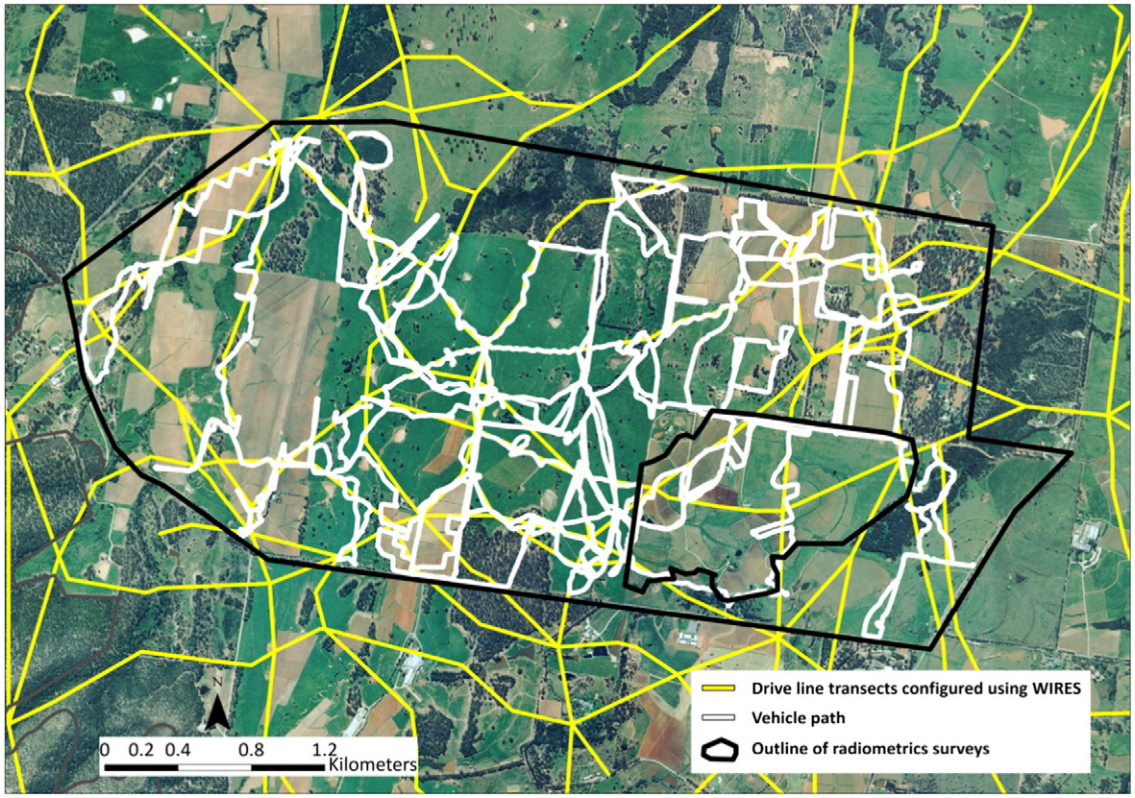

Fig. 6. Drive line transects of the regional-scale survey configured using WIRES. The vehicle path used to take proximal soil sensing measurements is also shown.

Table 1
Environmental covariates used in the step-wise multiple linear regression models. Terrain attributes were derived from a digital elevation model on a 25 m raster using the open source Geographic Information System SAGA. Detailed descriptions of the delineation of the soil physical and chemical properties can be found in Malone et al. (2014).

Total Counts (cps)	Potassium (cps)	Uranium (cps)	Thorium (cps)
Environmental covariates			
Eastings and northings	Eastings and northings	Eastings and northings	Eastings and northings
Clay content subsoil	Clay content subsoil	pH subsoil	Clay content subsoil
pH subsoil	pH subsoil	Analytical hillshading	pH subsoil
Analytical hillshading	Analytical hillshading	Altitude above channel network	Analytical hillshading
Altitude above channel network	Altitude above channel network	Aspect	Altitude above channel network
Aspect	DEM	DEM	DEM
DEM	Gamma radiometric total count	Gamma radiometric total count	Gamma radiometric total count
Gamma radiometric total count	mid-slope position	Planar curvature	mid-slope position
mid-slope position	Planar curvature	Profile curvature	Planar curvature
Planar curvature	Profile curvature	Compound topographic index	Profile curvature
Profile curvature	Compound topographic index	Slope	Compound topographic index
Slope	Slope	Terrain ruggedness index	Slope
Terrain ruggedness index	Terrain ruggedness index		Terrain ruggedness index

the regression is zero, simple kriging was used to interpolate the residuals. Interpolation was based on locally fitted variograms of the residuals, and kriging which was implemented using the VESPER software (Minasny et al., 2006). The regression predictions were added to the kriged residuals resulting in final (regression kriging) predictions of the radiometric target variables. Due to the number of data used for modelling in this study, the standard universal kriging algorithms were computationally unfeasible. Consequently we opted for the more computationally efficient regression modelling, then treatment of the residual type procedure. The advantage of this process for this particular study was that we were able to investigate the spatial structure of the residuals via locally fitted variogram models. Subsequently to derive 95% prediction intervals for each target variable, we estimated the overall standard error of the regression kriging predictions by taking the square root of the summed prediction variances (s^2) from both, the MLR model and kriged residuals. The standard error at each grid cell was used to calculate the subsequent 95% prediction limits.

To test the model performances, we split our dataset in a validation and calibration dataset (refer to Fig. 7). We left out 30% of the total number of 13 transects that have been surveyed to be included in the validation dataset which equated to 20% of the total radioelement sampling points. We then used the statistical measures of the R^2 and RMSE (root mean square error) to assess the accuracy of the predictions, and the prediction interval coverage probability (PICP), which is described in Malone et al. (2011), as an accuracy assessment of the associated uncertainties.

Another assessment of the quality of the estimated radiometric maps was to compare them with existing fine-resolution radiometric maps (refer to Fig. 5) surveyed for the intention of precision soil

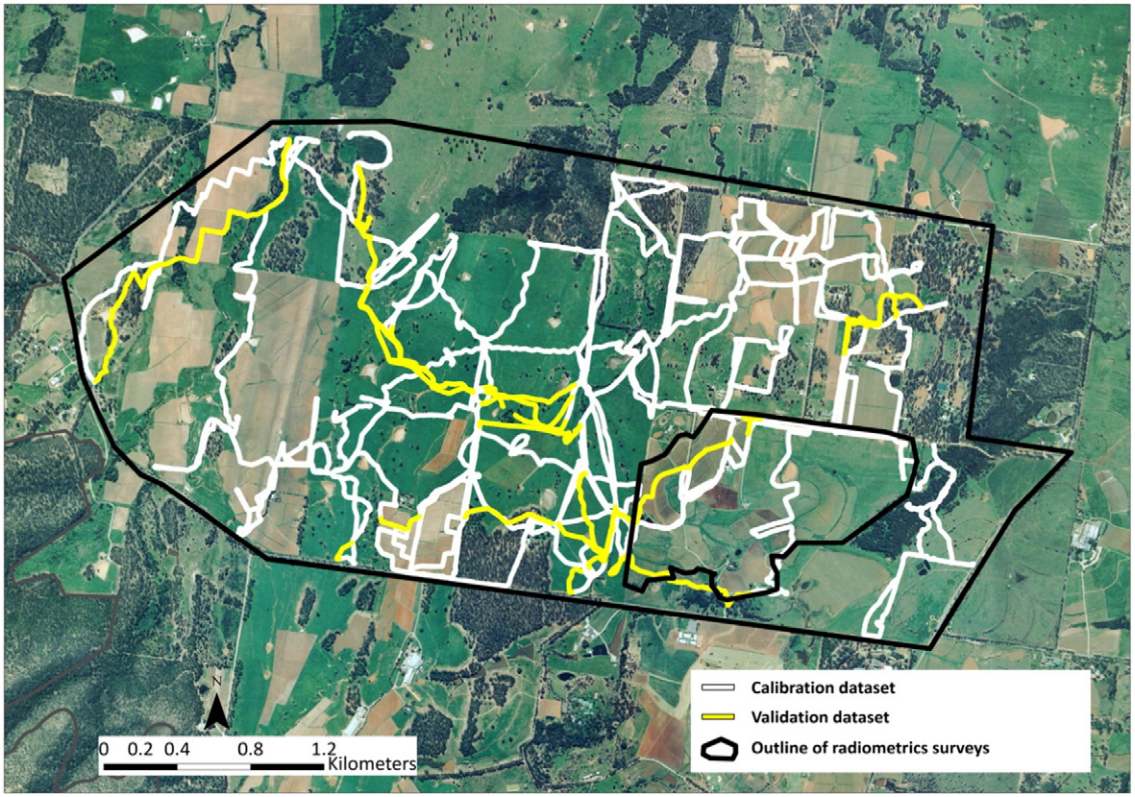

Fig. 7. Calibration and validation dataset used in the digital soil mapping prediction.

management across a landholding of approximately 140 ha in autumn 2012. This landholding is located within the WIRES surveyed sub-catchment (Stockmann et al., 2012). These fine-scale maps (10 m grid resolution) of the ROI were derived from a detailed ground survey of 30 m drive-line spacing (with a sampling density of 278 sampling points per hectare) using ordinary point kriging from locally fitted variograms. The resultant kriging prediction variances were used to estimate the 95% prediction intervals at each 10 m grid point.

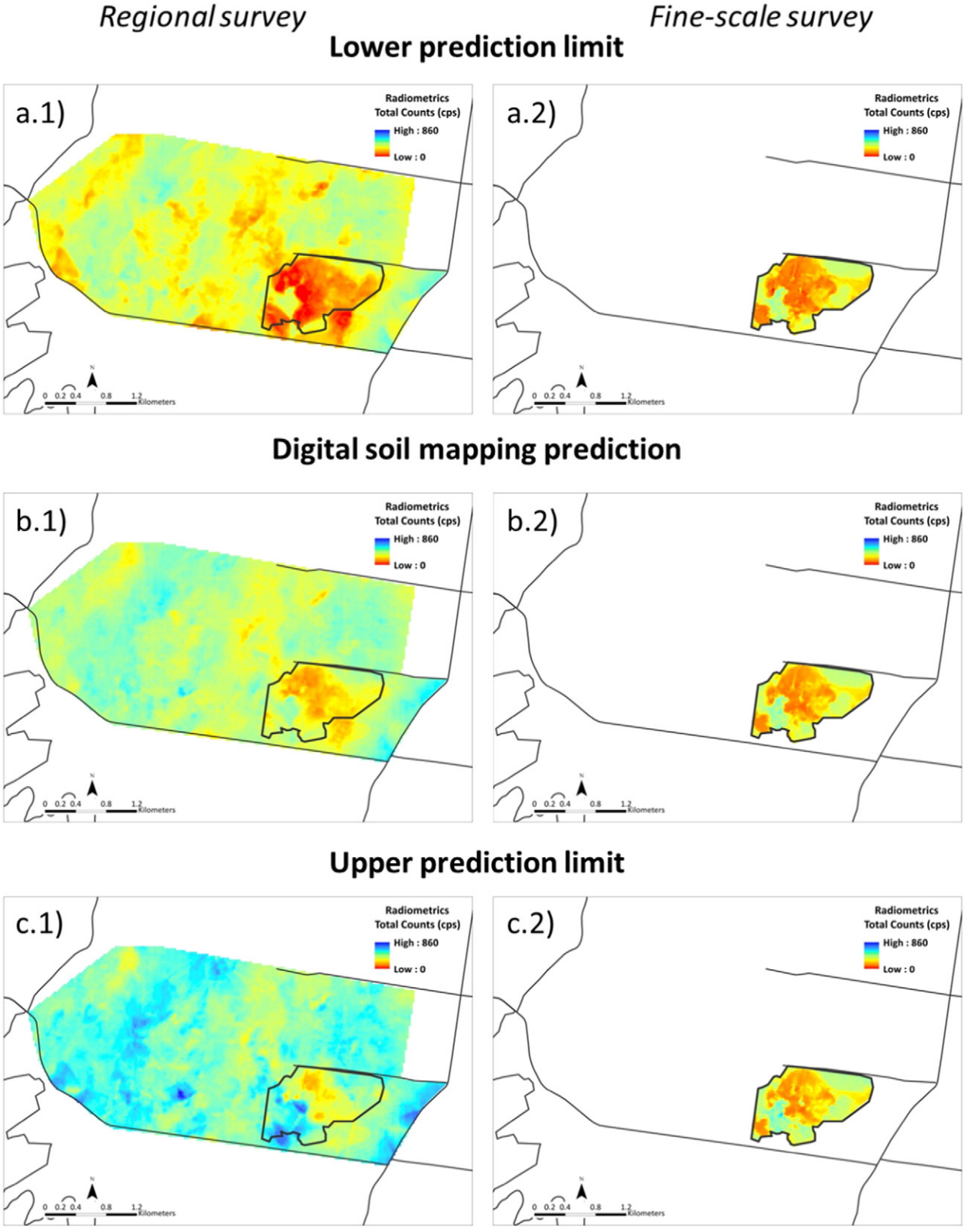

Fig. 8. Radiometric maps of the Total Counts (cps). The predictions generated using the regression kriging digital soil mapping approach of the regional survey (b.1) and the kriging approach of the fine-scale survey (b.2) are shown. In addition, the lower (a.1 and b.2) and upper (c.1 and c.2) predictions intervals (PI) are shown.

To compare the regional-scale 25 m resolution radiometric maps with those intended for precision land management (10 m resolution), we performed fine-gridding (using nearest neighbour re-sampling) of the regional-scale map predictions and their prediction limits to 10 m resolution (Malone et al., 2013). To compare the now equally resolved maps, we used the following four quantitative measures:

(1) PICP 1 — Prediction Interval Coverage Probability 1. This is a measure determining the percentage of points of the fine-scale

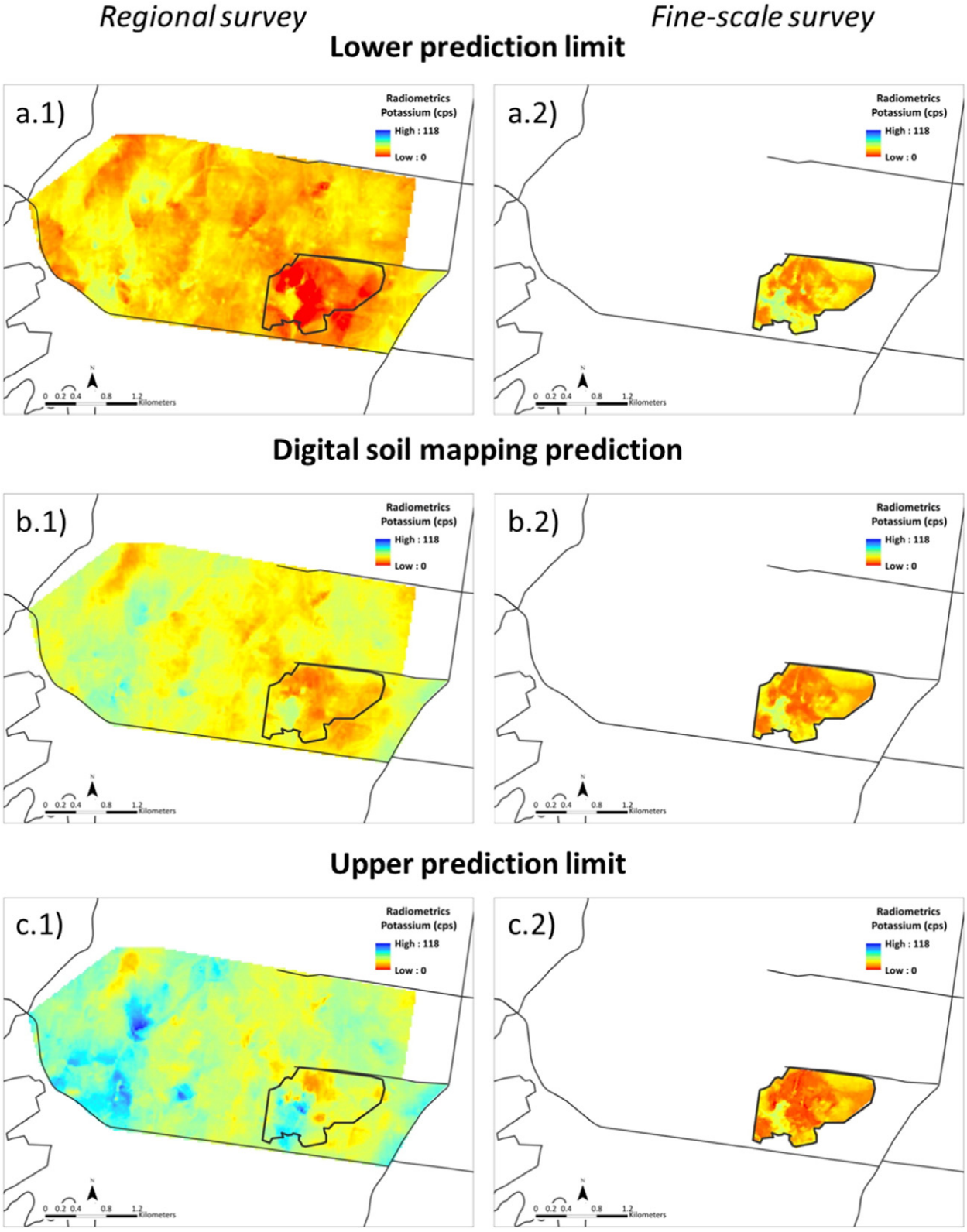

Fig. 9. Radiometric maps of Potassium (cps). The predictions generated using the regression kriging digital soil mapping approach of the regional survey (b.1) and the kriging approach of the fine-scale survey (b.2) are shown. In addition, the lower (a.1 and b.2) and upper (c.1 and c.2) prediction intervals (PI) are shown.

mapping where the predicted value (e.g. Fig. 8.b.2) falls within the upper and lower prediction limits of the regional survey (e.g. Fig. 8.a.1 and Fig. 8.c.1).

(2) PICP 2 — Prediction Interval Coverage Probability 2. Similar to PICP 1 except this measure calculates the percentage of points of the regional-scale mapping where the predicted value (e.g. Fig. 8.b.1) falls within the upper and lower prediction limits of the fine-scale mapping (e.g. Fig. 8.a.2 and Fig. 8.c.2).

(3) Zero enclosure. This measure estimates the percentage of points where in consideration of the prediction intervals of both fine-

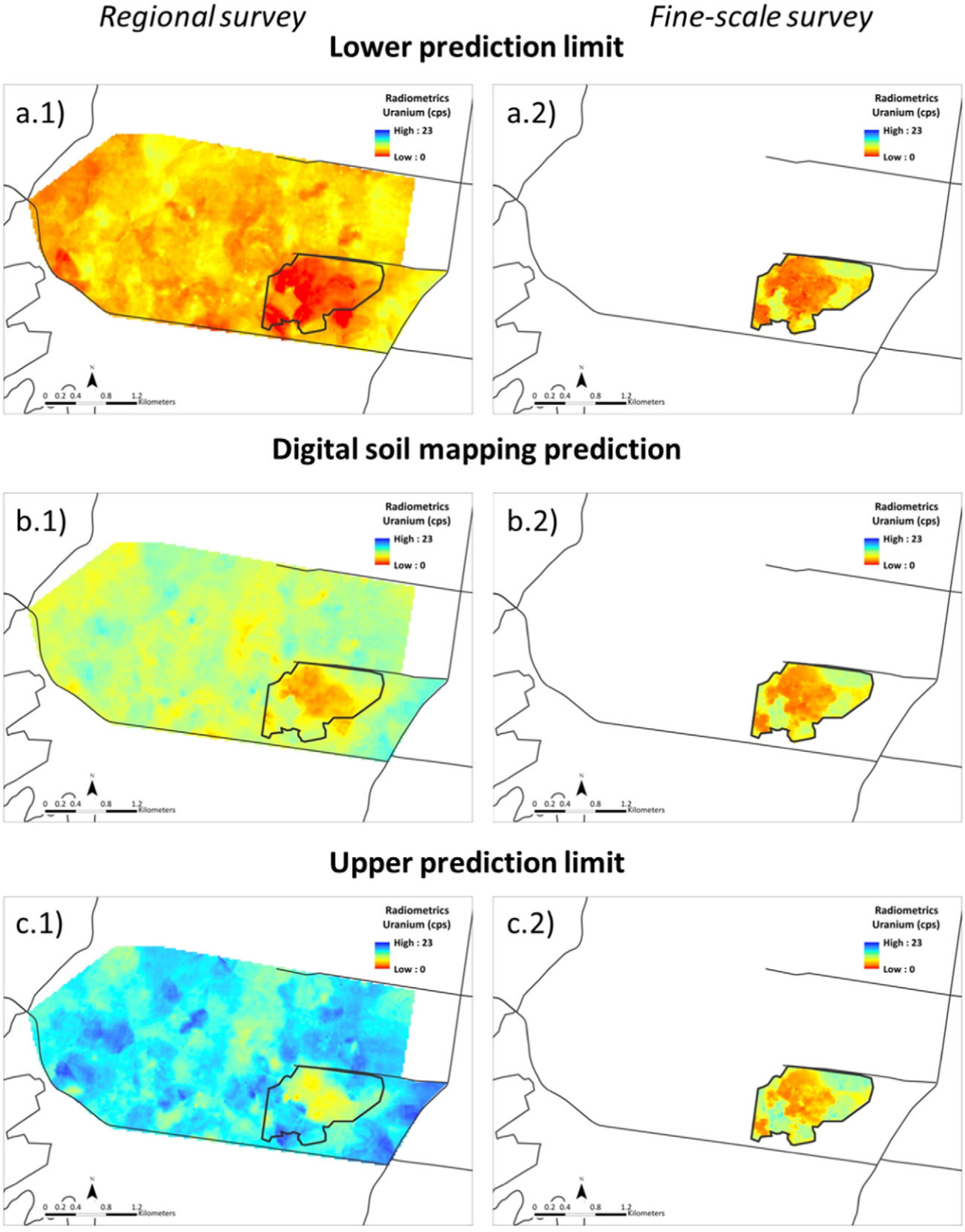

Fig. 10. Radiometric maps of Uranium (cps). The predictions generated using the regression kriging digital soil mapping approach of the regional survey (b.1) and the kriging approach of the fine-scale survey (b.2) are shown. In addition, the lower (a.1 and b.2) and upper (c.1 and c.2) prediction intervals (PI) are shown.

scaled (e.g. Fig. 8.a.2 and Fig. 8.c.2) and regional-scaled mapping (e.g. Fig. 8.a.1 and Fig. 8.c.1), there is no overlap. A value closer to zero is ideal as this means that the predictions (with associated uncertainties) have some overlap.

(4) SMDR — Simulated mean distance of realisations. This is a standardised mean distance measure of randomly simulated values from the distributions at each point from both regional- and fine-scaled surveys. Taking into account the prediction

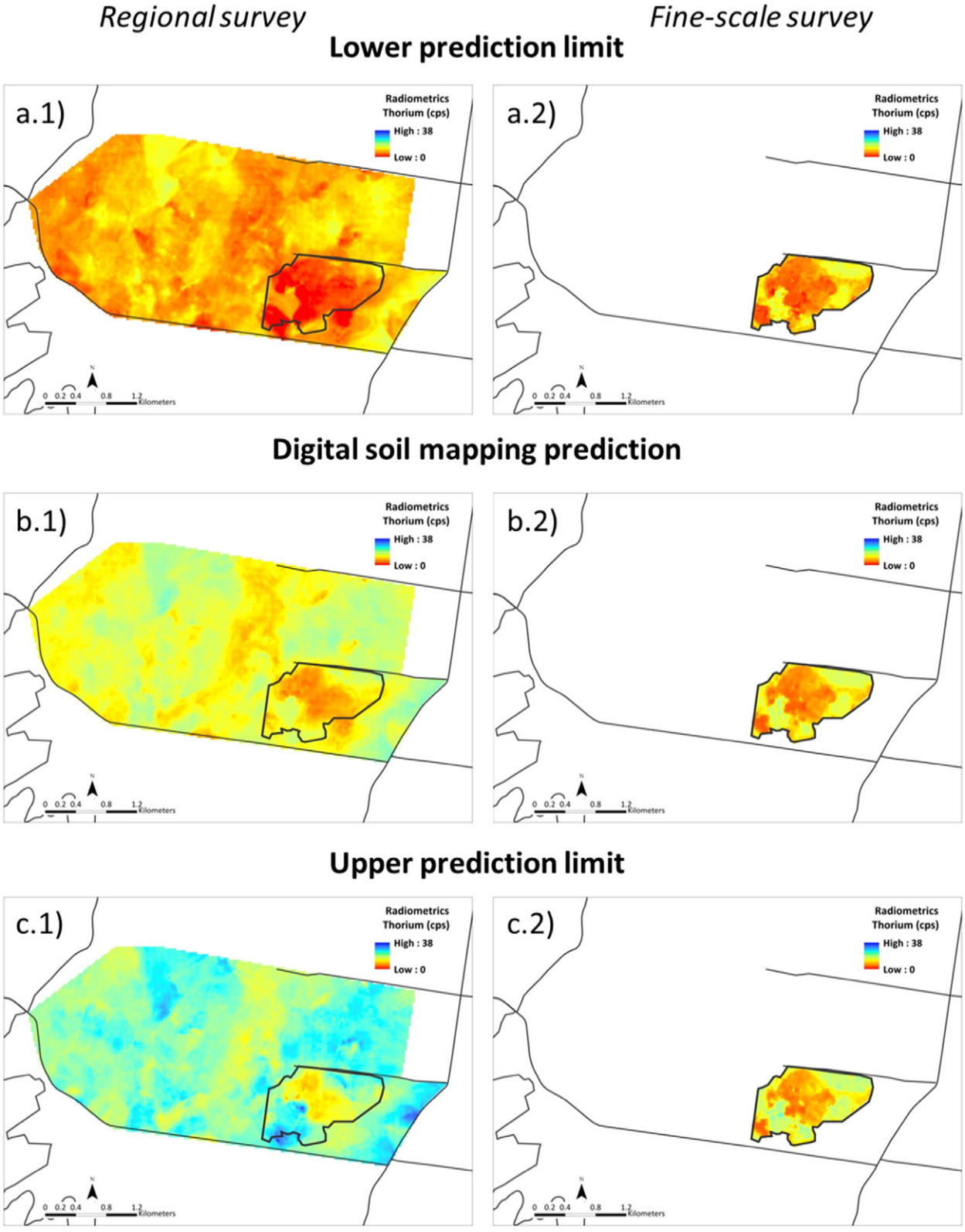

Fig. 11. Radiometric maps of Thorium (cps). The predictions generated using the regression kriging digital soil mapping approach of the regional survey (b.1) and the kriging approach of the fine-scale survey (b.2) are shown. In addition, the lower (a.1 and b.2) and upper (c.1 and c.2) prediction intervals (PI) are shown.

Table 2
Validation statistics from regression models with covariate information alone and regression kriging models for each of the studied ROIs.

ROI	Regression model		Regression kriging model		
	R^2	RMSE	R^2	RMSE	PICP
Total Count	0.38	71.44	0.54	60.73	88
Potassium	0.26	9.54	0.40	8.56	90
Thorium	0.23	3.92	0.35	3.60	92
Uranium	0.18	2.72	0.23	2.82	92

intervals, essentially for each radiometric map, at each point, a Latin Hypercube sample (n = 500) from the associated prediction distributions was taken. Each sample was scaled (according to the standard deviation), and then the standardised Euclidean distance calculated between the two simulated values. The mean of all the Euclidean distance realisations was the measure of SMDR at the subsequent point. Maps of the SMDR for each radiometric map were produced (Fig. 12), where values close to zero indicate similarity between regional-scaled and fine-scaled predictions. Alternatively, the higher the value, the less similar the predictions between both surveys.

3. Results and discussion

3.1. Implementation of WIRES in the field

It would be useful to have some additional information about the cadastral units of the study area to improve the implementation of the WIRES-informed regional radiometrics survey in the field. For instance, knowledge of the location of gates along fence lines (where in place) would improve the efficiency of delineating the vehicle path in the field and therefore reduce the surveying time significantly. However, the need for adjusting the vehicle path during the survey and not knowing readily how to proceed with arriving back onto the WIRES-delineated drive-lines was not necessarily an impediment as continuous radiometric readings were taken. Therefore, radiometric information of the studied landscape was still acquired which ultimately was the overall purpose of this proximal soil sensing survey.

3.2. Radiometric maps derived based on WIRES-delineated sampling points

Radiometric maps of the regional survey produced using regression kriging based on soil observations acquired through the WIRES drive line transects are shown in Fig. 8a.1–c.1 (Total Counts), Fig. 9a.1–c.1 (Potassium), Fig. 10a.1–c.1 (Uranium) and Fig. 11a.1–c.1 (Thorium). In addition, the environmental covariates used in the multiple linear regression models can be found in Table 1. Validation statistics are reported in Table 2. Here, we report validation statistics from regression models with covariate information alone and regression kriging models for each of the studied ROIs. Adding the kriged residuals improved predictions noticeably as these introduced additional and useful spatial structure which was unable to be modelled using the environmental covariates only. Spatial radiometric patterns seen in Figs. 8 to 11 are thus mainly inherited in the kriged residuals.

Regression kriging modelling of radiometric total counts was the best overall where an R^2 of 0.54 was observed. It was to be expected that this model to be the best performing as the total count is an integrated value of the gamma-radiometric spectrum, rather than a specific ROI as for the other variables. The quantifications of uncertainty for total

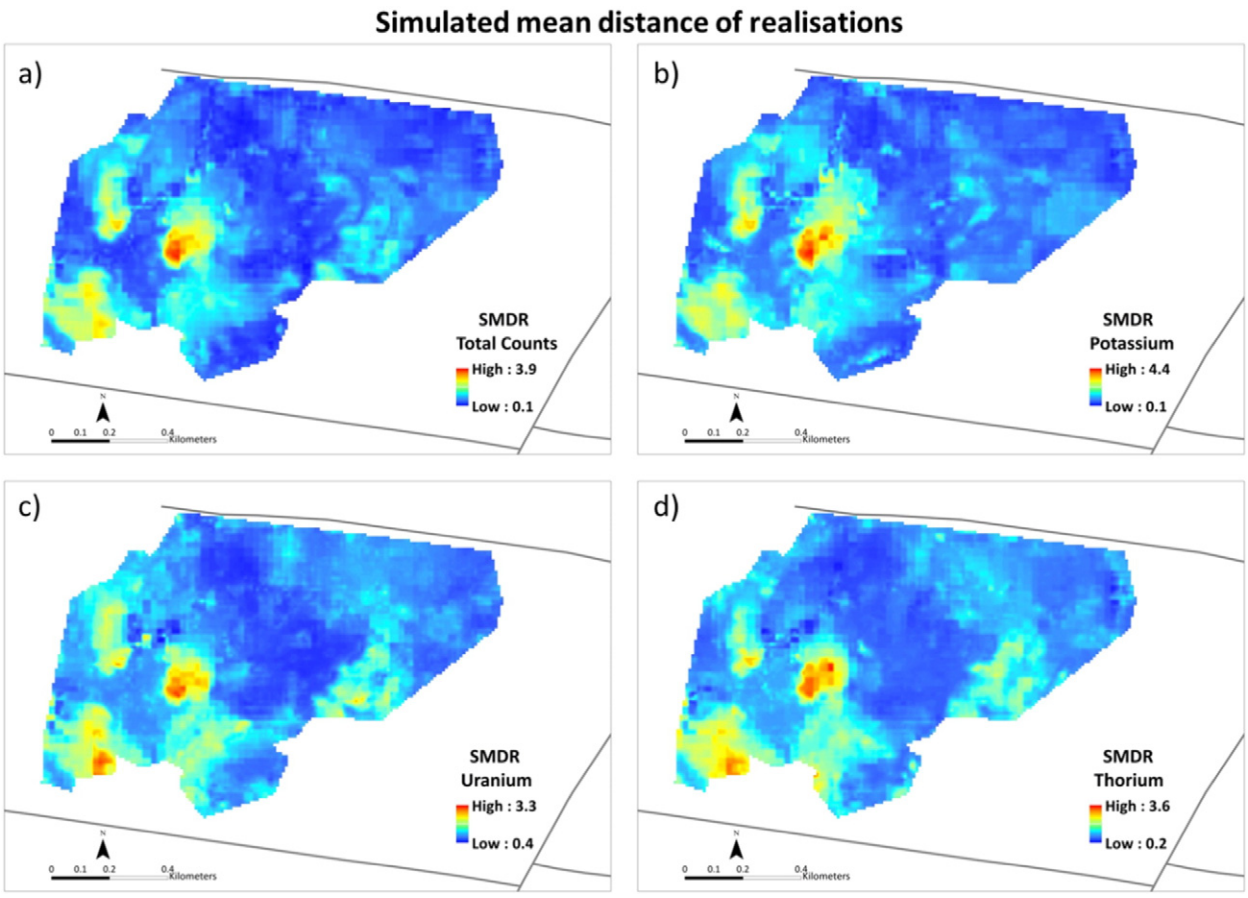

Fig. 12. Maps of the simulated mean distance of realisations (SMDR) for each radiometric map, Total Counts (a), Potassium (b), Uranium (c) and Thorium (d). Values close to zero indicate similarity between the regional- and fine-scaled predictions. On the other hand, the higher the value, the less similar the predictions between both surveys.

count seem acceptable with a PICP of 88%, although the expectation is for 95%. For the other ROIs, the validation R^2 was 0.40, 0.35, and 0.23 for potassium, thorium, and uranium respectively. The PICPs for each of the ROIs indicate that the quantifications of uncertainty are reasonable. Whilst we expected the performance of the modelling of these variables to be smaller than that for the total count, it is not uncommon in digital soil mapping to have R^2 values less than 0.5. Generally, such results indicate there to be a paucity of covariates that are available to explain the spatial variation of a given target variable (Malone et al., 2009; Odgers et al., 2011). Another factor contributing to the model uncertainty is the fact that the abundance of the individual radioelements in soil is low. This is particularly the case for uranium (Rogers and Adams, 1978), where there is often a low signal-to-noise ratio for its detection across the environment. Whilst there is future potential to improve the maps produced in this study as discoveries in remote and proximal sensing technologies are made, understanding the scaling properties of the radioelements will aid in predicting their spatial variation at any desired scale, irrespective of the scale to which the original data was acquired. Empirical studies relating detailed radiometric survey with more regional survey extent will be beneficial in that regard and should be investigated in future studies.

From what can be observed however from the produced regional scale radiometric maps, there is a clear spatial pattern of areas with low and high radiometric responses. These spatial patterns appear to be well supported by the ancillary information that we have of the study area such as the parent material's lithology. For instance, in the map of the Total Counts (Fig. 8a.1–c.1) as well as the maps of K (Fig. 9a.1–c.1), U (Fig. 10a.1–c.1) and Th (Fig. 11a.1–c.1), an area of very low counts in the lower left-hand side of the regional-scaled map is readily noticeable, surrounded by areas of (marginally) higher counts, which are most likely related to the change in parent materials the soils originated from. Low radiometric counts in this particular location of the study area are most definitely related to the carbonate-derived soils. Here, soils are underlain by marl — earthy deposits (indurated marine deposits from the Permian) consisting chiefly of an intimate mixture of clay and calcium carbonate. As discussed in Dickson and Scott (1997) carbonate-rich parent materials are known to be low in radioelements and in turn the soils formed from them are expected to have low radiometric responses. On the other hand, surrounding areas of higher radioelement content are most definitely related to sedimentary parent materials containing mudstone, claystone and shale that in general show a higher response in total radioelement content. During pedogenesis these geological units may have also experienced a proportional loss of K and the incorporation and concentration of U and Th into iron oxides and the fine fraction of soils (Dickson and Scott, 1997). Radiometric maps show a depletion of K and a slight increase of U and Th surrounding the Marl-derived soils, presumably due to the observed changes in radioelement concentrations inflicted by intense weathering.

Spatial patterns of increase in U and Th but loss in K across the whole study area are most definitely also related to clay-, as well as iron oxide and silt-rich soils or argillic units in general. U and Th as discussed above are associated with the fine fraction of soils that they weather into during pedogenesis. Conversely, low readings across the board are related to the abundance of sand-rich/coarse soil materials. These observed spatial patterns are in turn also related to the change in geological units across the study area, ranging from sandstone to siltstone, claystone and shale dominated parent materials.

As outlined earlier, we also compared the derived regional-scale radiometric maps with fine-scale radiometric maps from a small landholding in the survey area to investigate if WIRES is successful to also capture fine-scale soil heterogeneities. At first glance, the distinct pattern of high and low radiometric responses of the regional survey maps is (as expected) also clearly identifiable in the fine-scale survey maps (Fig. 8a.2–c.2, Fig. 9a.2–c.2, Fig. 10a.2–c.2, Fig. 11a.2–c.2), indicating that WIRES can be employed for the creation of drive-line transects for regional extent proximal soil surveys. However, to confidently argue that the soil's fine-scale heterogeneity can be captured, we performed a radiometric map quality assessment based on geostatistical approaches making use of several map quality indicators as outlined in Section 2.5 which will be discussed in the following.

3.3. Radiometric map quality assessment

First, it needs to be noted here that in the following, quality indicators are discussed with the view that the fine-scale radiometric mapping predictions reflect the soil's radioelement content more accurately. This notion is based on the fact that this proximal soil sensing survey was conducted on a very fine spatial resolution of 30 m (refer to McBratney and Pringle, 1999).

The radiometric map quality indicators confirm our conclusions made when interpreting the maps visually at first glance (Table 3 and Fig. 12), i.e. that WIRES is a reliable tool to be used for creating drive-line transects for regional scale radiometric surveys. For example, the

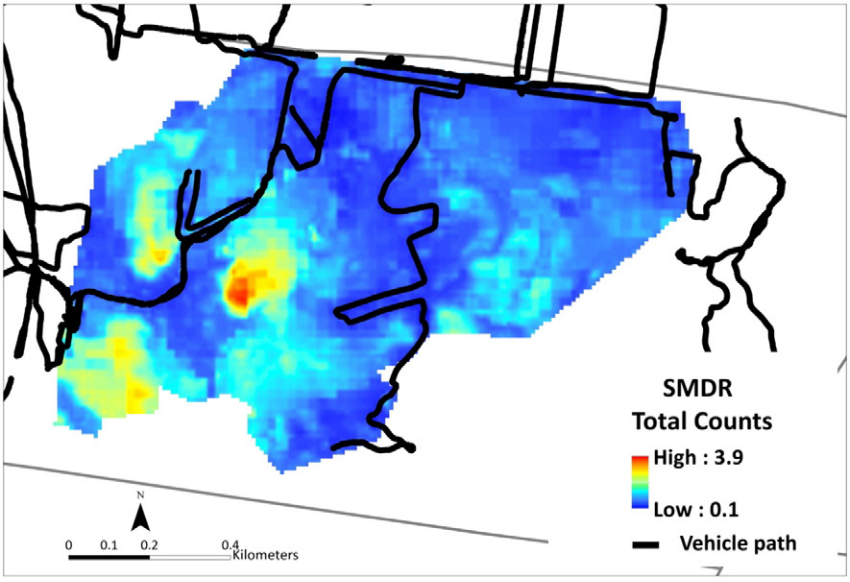

Fig. 13. Map of the simulated mean distance of realisations (SMDR) for the Total Counts including the vehicle path used to take proximal soil sensing measurements.

percentage of any point of the fine-scale mapping where the predicted value falls within the upper and lower prediction limits of the regional scale survey is relatively high (PICP 1), ranging from 88%, 94%, 96% and 98% for the Total Counts (cps), K (cps), Th (cps) and U (cps), respectively. On the other hand, the percentage of any point of the regional-scale mapping where the predicted value falls within the upper and lower prediction limits of the fine-scale survey is much lower (PICP 2), with 36%, 42%, 51% and 49% for the Total Counts (cps), K (cps), Th (cps) and U (cps), respectively, but still reasonable.

Cases of zero enclosure where there is no overlap (considering the prediction intervals) of both the fine-scaled and regional-scaled mapping are rare with a probability of less than 10% for all ROIs. The abundance of close to zero values therefore indicates that the predictions (with associated uncertainties) are more-or-less similar. All map quality indicators discussed here confirm or attest that intermediate wide-ranging drive lines of about 100 m in spacing width (and beyond) delineated using WIRES can still capture reasonably well the detail recorded by densely spaced drive lines of 30 m in width.

To assess the similarity of the regional-scale and fine-scale maps further and to visualize this measure, we calculated the scaled mean (Euclidean) distance of randomly simulated values from the distributions at each point from both surveys as outlined in Section 2.5, and subsequently called this measure the simulated mean distance of realisations (SMDR). Maps of the SMDR for each radiometric map show that generally the predictions between both surveys, fine- and regional-scaled, are relatively similar with most values close to zero (Fig. 12). Values larger than zero would indicate dissimilarity. However, there is a spatial pattern visible in all maps which identifies locations where the predictions between surveys are more similar than others. Additionally, one can also clearly locate regions in the SMDR maps of very high similarity. These regions of high similarity are (as expected) in similar locations for all radiometric maps (Fig. 12). More explicitly, comparatively low SMDR values are found in the centre and across the edges of the fine-scaled study area. These regions of high similarity seem to coincide with the transect locations of the regional-scaled survey. As can be seen in Fig. 13, high similarity occurs where vehicle-drive lines pass through the fine-scaled study area. This result may have been anticipated as one would expect the regions of drive-line transect cross-overs to be the most similar. However, this finding also attests that the gamma spectrometer that was used in both surveys is very reliable and consistent with measuring the soil's radioelement content of a location of interest.

4. Conclusions

The soil's passive gamma emissions are an invaluable asset for digital soil mapping. We have demonstrated in the work presented here that a 'smart' ground-based gamma radiometric survey can be an alternative when aerial radiometric information is not available at a desired resolution or not available at all. The sampling algorithm WIRES that was explicitly developed for this purpose proved to be successful in capturing fine scale soil heterogeneities as its implementation is based on ancillary information available for a location of interest. The successful implementation of WIRES was demonstrated using a range of radiometric map quality indicators which all confirmed that the radiometric map predictions (with associated uncertainties) from the regional-scaled and fine-scaled survey are more-or-less similar. We can therefore conclude that surveying a location of interest using optimal wide-ranging transects (≥100 m transect width) is sufficient enough to capture the soil's (heterogenic) radioelement concentration, and that a detailed fine-scale, high resolution survey (30 m transect width) may not be required to be able to measure the variability of soil attributes.

Table 3
Results of the radiometric map quality indicators (PICP = prediction interval coverage probability).

ROI, cps	PICP 1	PICP 2	Zero enclosure
Total Count	0.88	0.36	0.06
Potassium	0.94	0.42	0.03
Thorium	0.96	0.51	0.01
Uranium	0.98	0.49	0.00

Acknowledgements

We acknowledge the support of the Australian Research Council through its Discovery Program DP140102283 — A general soil spatial scaling theory. We would also like to thank three anonymous reviewers for their very useful comments on an earlier version of this manuscript.

References

Cattle, S.R., Meakin, S.N., Ruszkowski, P., Cameron, R.G., 2003. Using radiometric data to identify aeolian dust additions to topsoil of the Hillston district, western NSW. Soil Res. 41 (8), 1439–1456.
Cook, S., Corner, R., Groves, P., Grealish, G., 1996. Use of airborne gamma radiometric data for soil mapping. Soil Res. 34 (1), 183–194.
de Gruijter, J.J., Brus, D.J., Bierkens, M.F.P., Knotters, M., 2006. Sampling for Natural Resource Monitoring. Springer-Verlag, Berlin, Heidelberg.
Dickson, B.L., Scott, K.M., 1997. Interpretation of aerial gamma-ray surveys: adding the geochemical factors. AGSO J. Aust. Geol. Geophys. 17 (2), 187–200.
Filzmoser, P., Reimann, C., 2003. Multivariate outlier detection in exploratory geochemistry. Technical Report TS 03-5. Department of Statistics, Vienna University of Technology, Austria.
Glen, R.A., Beckett, J., 1993. Hunter Coalfield Regional Geology 1:100 000. Geological Survey of New South. Wales, Sydney.
Hawley, S.P., Glen, R.A., Baker, C.J., 1995. Newcastle Coalfield Regional Geology 1:100 000. 1st ed. Geological Survey of New South Wales, Sydney, Australia.
IAEA, International Atomic Energy Agency, 2003. Guidelines for Radioelement Mapping Using Gamma Ray Spectrometry Data, Vienna, Austria.
IUSS Working Group WRB, 2007. World Reference Base for soil resources 2006, first update 2007. World Soil Resources Reports No. 103. FAO, Rome.
Kovac, M., Lawrie, J.W., 1991. Soil Landscapes of the Singleton 1:250.000 Sheet. Soil Conservation Service of NSW, Sydney, Australia.
Malone, B.P., McBratney, A.B., Minasny, B., Laslett, G.M., 2009. Mapping continuous depth functions of soil carbon storage and available water capacity. Geoderma 154 (1–2), 138–152.
Malone, B.P., de Gruijter, J.J., McBratney, A.B., Minasny, B., Brus, D.J., 2011. Using additional criteria for measuring the quality of predictions and their uncertainties in a digital soil mapping framework. Soil Sci. Soc. Am. J. 75, 1032–1043.
Malone, B.P., McBratney, A.B., Minasny, B., 2012. Digital mapping of a soil drainage index in the Lower Hunter Valley, NSW. Proceedings of the Joint SSA and NZSSS Soil Science Conference – Soil solutions for diverse landscapes – 2–7 December 2012. Hobart, Tasmania.
Malone, B.P., McBratney, A.B., Minasny, B., 2013. Spatial scaling for digital soil mapping. Soil Sci. Soc. Am. J. 77 (3), 890–902.
Malone, B.P., Hughes, P., McBratney, A.B., Minasny, B., 2014. A model for the identification of terrons in the Lower Hunter Valley, Australia. Geoderma Reg. 1, 31–47.
McBratney, A.B., Pringle, M.J., 1999. Estimating average and proportional variograms of soil properties and their potential use in precision agriculture. Precis. Agric. 1 (2), 125–152.
McBratney, A.B., Mendonca Santos, M.L., Minasny, B., 2003. On digital soil mapping. Geoderma 117 (1–2), 3–52.
Minasny, B., McBratney, A.B., 2006. A conditioned Latin hypercube method for sampling in the presence of ancillary information. Comput. Geosci. 32, 1378–1388.
Minasny, B., McBratney, A.B., Whelan, B.M., 2006. VESPER, Version 1.6. Australian Centre for Precision Agriculture. http://sydney.edu.au/agriculture/pal/software/vesper.shtml.
Minty, B.R.S., McFadden, P., Kennett, B.L.N., 1998. Multichannel processing for airborne gamma-ray spectrometry. Geophysics 63 (6), 1971–1985.
Minty, B., Franklin, R., Milligan, P., Richardson, M., Wilford, J., 2009. The radiometric map of Australia. Explor. Geophys. 40 (4), 325–333.
Odeh, I.O.A., McBratney, A.B., Chittleborough, D.J., 1995. Further results on prediction of soil properties from terrain attributes: heterotopic cokriging and regression-kriging. Geoderma 67 (3–4), 215–226.
Odgers, N.P., McBratney, A.B., Minasny, B., 2011. Bottom-up digital soil mapping. II. Soil series classes. Geoderma 163 (1–2), 30–37.
Percival, P.J., 2010. Index of airborne geophysical surveys, Geoscience Australia, Record 2010/1311th ed. .
R Development Core Team, 2008. R: A Language and Environment for Statistical Computing. R Foundation for Statistical Computing, Vienna, Austria (ISBN 3-900051-07-0, URL http://www.R-project.org).
Rogers, J.J.W., Adams, J.A.S., 1978. Uranium (92), Thorium (90). In: Wedepohl, K.H. (Ed.), Handbook of Geochemistry. Springer-Verlag, Berlin.
Scheib, C., Beamish, D., 2010. High spatial resolution observations of ^{137}Cs in northern Britain and Ireland from airborne geophysical survey. J. Environ. Radioact. 101 (9), 670–680.

Stabile, M., 2011. Deconstructing the complexity of land use and cover classification and land change modelling, University of Sydney, Unpublished PhD Thesis.
Stockmann, U., Minasny, B., McBratney, A.B., Hancock, G.R., Willgoose, G.R., 2012. Exploring short-term soil landscape formation in the Hunter Valley, NSW, using gamma ray spectrometry. In: Minasny, B., Malone, B.P., McBratney, A. (Eds.), Digital Soil Assessments and Beyond. 5th Global Workshop on Digital Soil Mapping. CRC Press, Sydney, NSW, pp. 77–82.
Taylor, M.J., Smettem, K., Pracilio, G., Verboom, W., 2002. Relationships between soil properties and high-resolution radiometrics, central eastern Wheatbelt, Western Australia. Explor. Geophys. 33 (2), 95–102.
Viscarra Rossel, R.A., Taylor, H.J., McBratney, A.B., 2007. Multivariate calibration of hyperspectral γ-ray energy spectra for proximal soil sensing. Eur. J. Soil Sci. 58 (1), 343–353.
Viscarra Rossel, R.A., Webster, R., Kidd, D., 2014. Mapping gamma radiation and its uncertainty from weathering products in a Tasmanian landscape with a proximal sensor and random forest kriging. Earth Surf. Process. Landf. 39 (6), 735–748.
Wilford, J., 2012. A weathering intensity index for the Australian continent using airborne gamma-ray spectrometry and digital terrain analysis. Geoderma 183–184, 124–142.
Wilford, J., Minty, B., 2006. The use of airborne gamma-ray imagery for mapping soils and understanding landscape processes. In: Lagacherie, P., McBratney, A.B., Voltz, M. (Eds.), Developments in Soil Science. Elsevier, pp. 609–610.
Wilford, J.R., Bierwirth, P.N., Craig, M.A., 1997. Application of airborne gamma-ray spectrometry in soil/regolith mapping and applied geomorphology. AGSO J. Aust. Geol. Geophys. 17 (2), 201–216.